Industrial Implementation of Plasma Deposition Using the Expanding Thermal Plasma Technique

M.C.M. van de Sanden, P.J. van den Oever, and M. Creatore, Department of Applied Physics, Equilibrium and Transport in Plasmas, Eindhoven University of Technology, Eindhoven, The Netherlands; M. Schaepkens, T. Miebach, and C.D. Iacovangelo, General Electric Global Research Center, Schenectady, New York; R.C.M. Bosch, M. Bijker, and M. Evers, OTB Engineering B.V., Eindhoven, The Netherlands; and D.C. Schram and W.M.M. Kessels, Department of Applied Physics, Equilibrium and Transport in Plasmas, Eindhoven University of Technology, Eindhoven, The Netherlands

Key Words: Expanding thermal plasma; Silicondioxide, siliconnitride; Scratch resistant coatings; Antireflection coatings

ABSTRACT

Two successful industrial implementations of the expanding thermal plasma setup, a novel plasma source, obtaining high deposition rate are discussed. The Ar/O_2/hexamethyldisiloxane and Ar/O_2/octamethyl-cyclosiloxane-fed expanding thermal plasma setup is used to deposit scratch resistant silicone films on polycarbonate with the purpose of replacing glass by polymers in the architectural and transportation industry. Antireflection and bulk passivation coatings for crystalline silicon solar cells based on silicon nitride films and deposited from $Ar/N_2/SiH_4$ and $Ar/NH_3/SiH_4$ mixture are discussed next. It is shown that the versatile control of parameters in the ETP setup (i.e., arc current, gas flow rates and working pressure) enable specific tuning of the film properties (i.e., chemical composition, optical and mechanical properties).

INTRODUCTION

Plasma deposition of thin films has specific advantages over other physical or chemical vapor deposition techniques because the dissociation of deposition precursors takes place in the gas phase, enabling the deposition of thin films on relatively cold substrates. Furthermore, the additional presence of ion bombardment, due to the difference in electron and ion mobility, enables the formation of high quality films since the surface mobility of deposition precursors can be enlarged, and thus allowing the surface and bulk morphology to be controlled. Usually plasma deposition also leads to higher deposition rates than physical and chemical vapor deposition techniques. These relative advantages have made plasma deposition the first choice in high value added industries such as the semiconductor industry. However, the deposition rates are usually rather low (< 1 nm/s), hampering the application of plasma deposition in large scale low added value applications such as barrier coatings on polymer substrates, thin film solar cells, or scratch resistant coatings on polymer glazing. A fast plasma deposition technology which enables the deposition of high quality dense coatings would open up new markets for the application of plasma deposition technology. In this paper we discuss the successful implementation of the expanding thermal plasma (ETP) deposition technology for the high rate deposition of scratch resistant $SiO_xC_yH_z$ coatings on polymer substrates and a-SiN_x:H as antireflective coatings on multi-crystalline solar cells. These are only two examples of the films deposited using the ETP technology. Other successful classes of thin films deposited at high rate using the ETP technology are a-Si:H [1], a-C:H [2] and ZnO [3].

THE EXPANDING THERMAL PLASMA

The expanding thermal plasma (ETP) technique, invented almost two decades ago, combines a high-pressure plasma source with a low-pressure processing (deposition) reactor [4] (see Figure 1a). The plasma source is a cascaded arc in which a plasma is generated by the application of a dc voltage to typically three cathodes that arc to one common grounded anode through a nondepositing carrier gas flowing through a narrow channel (see Figure 1b). This carrier gas is often Ar but also H_2, N_2 or mixtures of these gases can be used. Due to the narrow channel, high gas flows and the plasma itself, the pressure in the plasma source is subatmospheric (typically 400 mbar) which means that the plasma is thermal. The electron and ion density in the channel is about 10^{15} cm^{-3}, and due to the local thermal equilibrium, the electron, ion, and gas temperature are equal and about 1 eV. The plasma expands through a nozzle into the low-pressure reactor and due to the pressure difference the expansion is first supersonic, and after a stationary shock front (typically at ~5 cm from the nozzle at 0.2 mbar background pressure), subsonic. Due to the expansion behavior, the electron temperature as well as the electron and ion density is significantly reduced in the downstream region. The downstream electron temperature is typically 0.1-0.3 eV depending on the gases used and therefore electron induced dissociation and ionization reactions can be neglected in the downstream region different from conventional plasma techniques. The downstream ion density, on the other hand, is relatively high (10^{13} cm^{-3} for pure Ar down to 10^{11} cm^{-3} for molecular plasmas) compared to other plasma techniques, and this can be attributed to the fact that plasma creation takes place in a source at high-pressure with consequently a much higher ionization degree than for low-pressure plasmas. Furthermore, when molecular gases such as H_2 and N_2 are admixed in the source, the frequent electron collisions and the high gas temperature cause a very high dissociation degree of the gases. This leads to large fluxes of H and N atoms from the source and, due to very effective dissociative ion-electron recombination reactions in the expansion zone for molecular gases, the plasma source operates under these

conditions predominantly as an atomic H or N source (with the atom density typically a factor 10-100 higher than the ion density). Consequently, the high-pressure plasma source delivers very large flows of ions (Ar^+) or atoms (H, N) to the downstream region, and therefore a large amount of “reactivity” to precursor gases such as NH_3 and SiH_4 that are injected downstream in the reactor. Due to the low electron temperature, these precursor gases are dissociated by ionic and/or atomic reactive species, and due to the large amount of “reactivity” also much larger flows of precursor gases [(the flows are typically in the order of 1 standard liter per minute (slm)] can be dissociated than in conventional low-pressure plasmas. Two other important advantages of the ETP technique are that a relatively selective chemistry (e.g., precursor gas dissociation by Ar^+ or H by the selection of the carrier gas) can be chosen in contrast to electron-collision dominated plasmas, and the fact that the source operation is not influenced at all by the downstream region (i.e., the ETP is the ultimate “remote plasma”). The latter aspect enables independent optimization of the upstream and downstream plasma region. The low pressure in the downstream region (generally 0.2 mbar, similar to typical pressures in rf parallel plate reactors) prevents excessive gas phase polymerization reactions and therefore abundant dust formation. Furthermore, the low electron temperature leads to very low substrate self-bias voltages, although additional rf substrate biasing can be applied to generate a controllable level of ion bombardment.

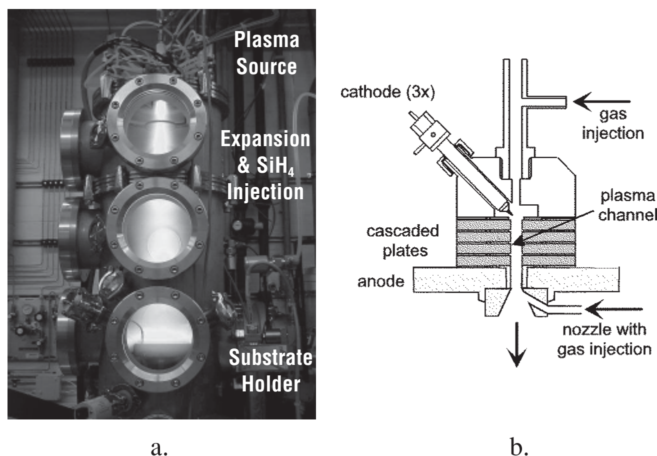

Figure 1: a.) Expanding Thermal Plasma (ETP) setup, and b.) schematic of the ETP plasma source (i.e., cascaded arc).

Within the last decade the ETP technique has been applied for the deposition of thin films of all kind of materials such as carbon [2] and silicon [3] films (amorphous, nanocrystalline, and diamond-like), oxides (silicon oxide [5] and zinc oxide [3]), and nitrides (carbon nitride and silicon nitride [6]). Furthermore, in recent years several companies have licensed the ETP technology for particular applications with the two most important players, General Electric [7] and OTB Engineering B.V.

SCRATCH RESISTANT $SIO_XC_YH_Z$ COATINGS ON POLYMER SUBSTRATES

Recently, an interest has risen in the transportation and architectural industry to replace glass by polymeric materials. [7] Polymeric materials (e.g., polycarbonate) are equally transparent compared to glass but have the advantage of being light, flexible and rugged at the same time. However, in order to bypass the disadvantages of polymeric materials, i.e., UV sensitivity and scratch sensitivity, protective films are needed. In this contribution, the scratch resistant film is addressed. Such a film will modify surface properties of the polymer, in particular its tendency to be scratched, to ensure that the coated polymer is comparable to glass. For polycarbonate, the hardness/Young’s modulus is typically 0.2/4 GPa, whereas for glass these values are 5/75 GPa. Silicone ($SiC_xH_yO_z$) hardcoats have previously been applied to polycarbonate to accomplish increased scratch resistance using atmospheric wet coating technologies. Recently, alternative deposition techniques, such as chemical vapor deposition and plasma enhanced chemical vapor deposition (PECVD), have been developed for industrial applications because of their nonsolvent approach and good adhesion of the films to the polymeric substrate. In particular, a novel organosilicon-based PECVD technique based on an Ar/O_2/hexamethyldisiloxane (HMDSO) and Ar/O_2/octamethylcyclotetrasiloxane (D4) expanding thermal plasma (ETP) source. Specifically, this technique enables the fast deposition of active organosilicon species from the plasma gas phase onto the polymeric surface. Due to the versatile control parameters of the setup and the chemical/physical character of the PECVD technique, the properties of the silicone films (e.g., chemical composition, optical and mechanical properties) can be tuned to the specific applications at hand, as will be shown further on [5,7]. At General Electric Global Research Center, the ETP source is already being employed in an industrial fast, large area (multisource) deposition reactor for silicone films on polycarbonate (GE Lexan® MR 10).

O_2 is injected into the plasma through the nozzle and HMDSO and D4 are injected through a ring located at approximately five cm from the outlet of the arc. Due to the low electron temperature, electron-monomer dissociation pathways are unlikely and the dissociation of HMDSO is controlled by dissociative recombination pathways involving Ar^+ and low energy electrons. The reactions in Equation 1 show the possible dissociation of HMDSO molecules in the expanding thermal plasma [5]: a charge exchange occurs between the Ar^+ and the HMDSO molecule and subsequently, the HMDSO molecule can dissociate (dissociative recombination) at the Si-O, Si-C or C-H (Me = methyl group).

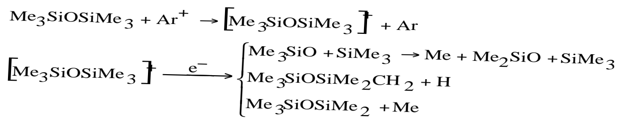

Equation 1

Mass spectrometry measurements are performed to determine which of the reactions in Equation 1 occur in the ETP setup. Figure 2a shows the depletion of the HMDSO molecule as a function of the arc current. In the same figure the Ar^+ flow rate, determined from Langmuir probe measurements [8], is also shown. It appears that the depletion of HMDSO molecule depends on the availability of Ar^+, which supports the charge exchange reaction in Equation 1. In Figure 1b the ratio of the fragment $Si(CH_3)_3^+$ (m/e=73 amu) and HMDSO (m/e=147 amu) intensities is shown as a function of the arc current, when the plasma is turned on and off. The fragment $Si(CH_3)_3^+$ is the parent ion of either the molecule $Si(CH_3)_4$ or the radical $Si(CH_3)_3$. A clear enhancement of the fragment is seen when the plasma is turned on, indicating that $Si(CH_3)_3^+$ is created in the plasma phase. Being the only fragment for which this enhancement is seen, it is suggested that the Si-O bond of the HMDSO molecule is broken, preferably in the ETP setup (second reaction in Equation 1), at least in conditions for which $[Ar^+] \cong [HMDSO]$. However, the breakage of the Si-O bond in the gas phase is not desirable as it represents the "mechanically strong" backbone for the deposition of scratch resistant $SiC_xH_yO_z$ films.

On the basis of the results mentioned above, in order to "rebuild" the strong SiOSi network, it is necessary to dilute the HMDSO in O_2. First, the influence of O_2 dilution on the gas phase is investigated in Figure 3. The depletion of HMDSO flow rate as a function of the depletion of O_2 flow rate shows that the influence of O_2 addition is negligible, meaning that the charge exchange of HMDSO with Ar^+ is preferred above charge exchange with O_2 ($O_2+Ar^+ \rightarrow O_2^+ + Ar$), which has a low reaction rate of (4.6 x 10^{-11} cm^3/s). The saturation of the depletion of O_2 depends on the limited availability of Ar^+. However, at this point we cannot exclude reactions of molecular oxygen with HMDSO fragments. Second, the film characteristics have been analyzed by means of spectroscopic ellipsometry. In Figure 4a the refractive index and the deposition rate of the film are shown as a function of the O_2 dilution. The increase of the deposition rate implies that O_2 affects the film growth, e.g. by reacting with HMDSO fragments. The details of the underlying mechanism will be studied in future work. The decrease of the refractive index to a value lower than the refractive index of SiO_2 ($\approx$1.46) implies that O_2 oxidizes carbon (film etching) and creates voids. In Figure 4b. the decrease of the imaginary part of the dielectric function at low wavelengths indicates a decrease in UV absorption by the film, which in turn is caused by carbon incorporated in the film.

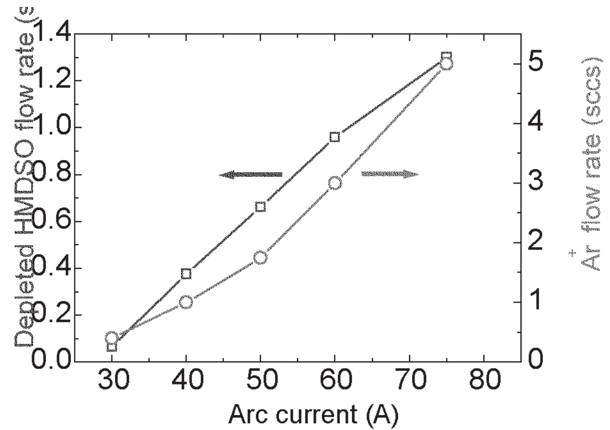

a.

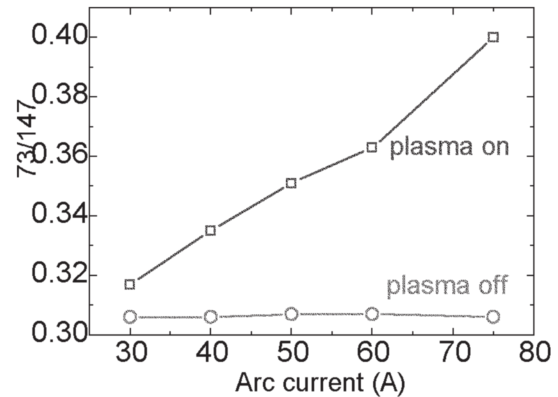

b.

Figure 2: a.) Mass spectrometry results of the depletion of the HMDSO molecule in comparison to the Ar^+ flow rate from the arc as a function of the arc current. b.) 73 amu intensity normalized to the HMDSO parent ion (147 amu) intensity as a function of the arc current, when the plasma is turned on and off. Other experimental conditions: Φ_{Ar}=25 sccs, I_{arc}=50 A, Φ_{HMDSO}=2 sccs, $p_{reactor}$=0.11 mbar.

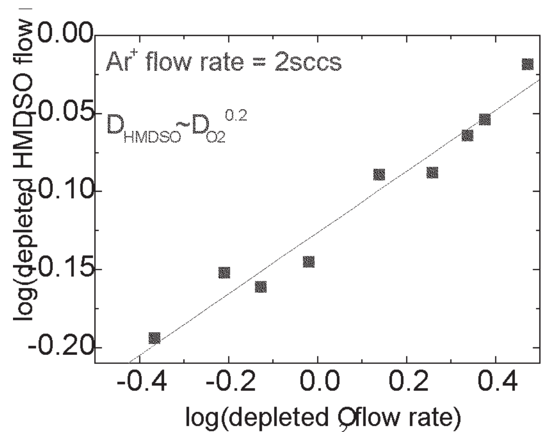

Figure 3: Mass spectrometry results of the depletion of the HMDSO flow rate as a function of the depletion of the O_2 flow rate. Other experimental conditions: Φ_{Ar}=25 sccs, I_{arc}=50 A, Φ_{HMDSO}=2 sccs, $p_{reactor}$=0.11 mbar.

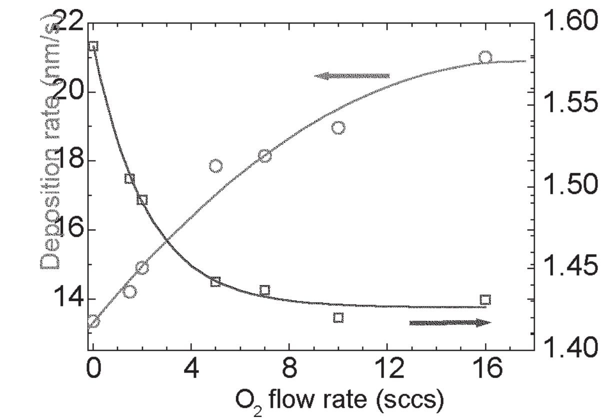

a.

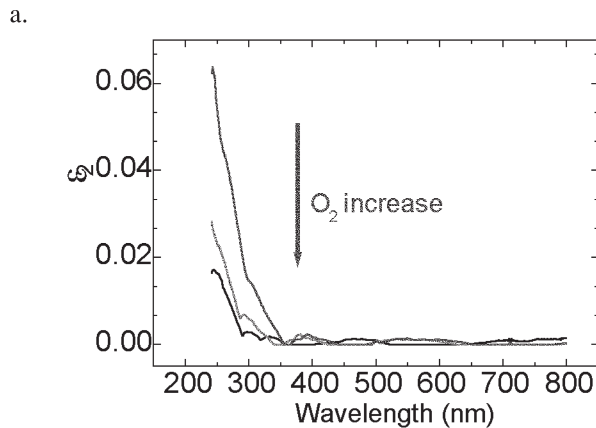

b.

Figure 4: a.) Spectroscopic ellipsometry results of the deposition rate and refractive index of the deposited films as a function of the O_2 flow rate in the gas phase. b.) Spectroscopic ellipsometry results of the imaginary part of the dielectric function as a function of the O_2 flow rate in the gas phase. Other experimental conditions: Φ_{Ar}=25 sccs, I_{arc}=50 A, Φ_{HMDSO}=2 sccs, $p_{reactor}$=0.11-0.16 mbar.

In order to realize a capable large area high-rate coating process, a reactor in which two ETP sources were carefully spaced at a distance corresponding to the effective width of the single-ETP process profile [7]. In addition, injection rings that would insure uniform gas injection around the two ETP sources were designed, constructed, and installed onto the dual-ETP source reactor. Deposition experiments in which $SiO_xC_yH_z$ coatings, which can serve as abrasion resistant coatings, are deposited from a mixture of D4 and oxygen on 45 cm x 45 cm polycarbonate substrates that were pre-coated with a silicone hardcoat (GE Lexan® MR10) were performed. The mixtures of D4 and oxygen were injected through a single injection ring that surrounds both ETP sources. Prior to deposition, the substrates were preheated to temperatures around 100°C. The substrates were translated in a single pass by the dual-ETP source array at a speed of 2.5 cm/s. The inner 30 cm x 30 cm area of the coated substrates, which had a coating thickness nonuniformity of less than 5% sigma/mean, were evaluated for abrasion resistance using the Taber abrasion method (ASTM D1044-94), i.e., the increase in haze was measured after ~1000 cycles of Taber abrasion using CS10F wheels with a 500 g load were performed. Figure 5 shows a typical abrasion resistance profile. For reference, we included the values of haze increase, i.e. delta haze, for both glass and silicon hardcoated polycarbonate substrates submitted to the same Taber abrasion test. It shows, in Figure 5, that near glass like abrasion resistance can be achieved uniformly across a width of 30 cm on ETP abrasion layer coated and silicone hardcoated polycarbonate substrates.

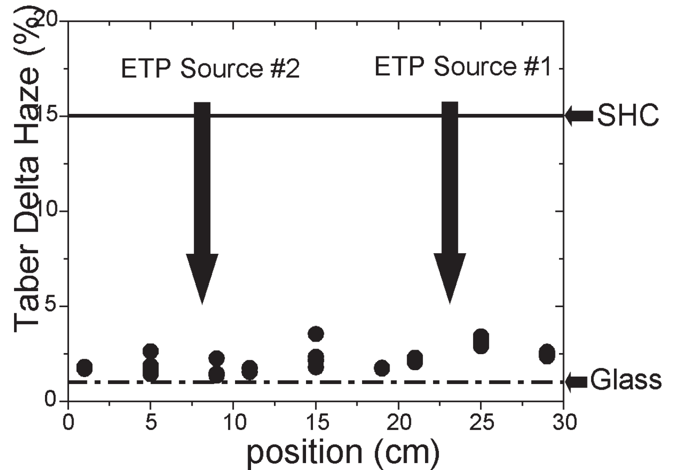

Figure 5: Profiles of the abrasion resistance performance of $SiO_xC_yH_z$ coatings are deposited with argon ETPs from a mixture of D4 and oxygen on to 100°C preheated polycarbonate substrates that were precoated with a silicone hardcoat and then translated by a dual-ETP source array. The abrasion resistance is evaluated by the Taber abrasion method (1000 cycles) and measured in terms of increase in haze of the substrate (i.e., Taber delta haze). For reference, we included the Taber delta haze values of nonplasma coated substrates (i.e., ~15%) and of glass (i.e. ~1%). The average Taber delta haze values of the current sample is ~2.2%.

ANTIREFLECTION COATINGS ON C-SI SOLAR CELLS

Silicon nitride films have been deposited by the ETP using the reactant mixtures N_2-SiH_4 and NH_3-SiH_4 [6]. When using the N_2-SiH_4 reactant mixture, an Ar-H_2-N_2 gas mixture is injected in the cascaded arc at a typically flow ratio of 3.3 slm : 0.3 slm : 0.6 slm and an arc current of 45 A. SiH_4 is injected in the downstream expansion zone by means of an injection ring at a typical flow up to 1 slm (1 slm is equivalent to 1000 sccm or about 16.7 sccs). For the NH_3-SiH_4 reactant mixture, the cascaded arc is operated on pure Ar while NH_3 is injected in the plasma through the nozzle (see Figure 1b) and SiH_4 through the injection ring. The Ar and NH_3 flows are typically 3.3 slm and 1 slm respectively, while the SiH_4 flow is typically varied between 0.05 and 0.3 slm. The arc current is within the

range of 45-75 A. For both types of plasmas, the downstream pressure is approximately 0.20 mbar. To study the material properties, the a-SiN_x:H films are deposited on different types of substrates (c-Si, mc-Si wafers) with a maximum size of 10 x 10 cm^2. The substrate temperature is actively controlled and is typically 400°C [6].

With both types of plasmas, a-SiN_x:H films can be deposited at very high deposition rates, i.e., up to 20 nm/s. However, in our experiments the films are typically deposited at a rate of ~5 nm/s [6]. A very important aspect of plasma deposition is that the refractive index of the a-SiN_x:H films can be accurately tuned by varying the SiH_4/N_2 or SiH_4/NH_3 flow ratio, as a good control of the refractive index is necessary to optimize the antireflection coating (ARC) performance of the a-SiN_x:H film. Depending on the solar cell and panel design, a refractive index of ~2.0 (at 2 eV) gives the best ARC performance in air while a refractive index of ~2.4 (at 2 eV) gives the best ARC performance behind glass [9,10]. As shown in Figure 6, the refractive index can be precisely tuned by operating the ETP at different flow mixtures. However, another requirement is that the absorption losses in the a-SiN_x:H are kept sufficiently low. When the refractive index is raised, the extinction coefficient of the a-SiN_x:H increases as also shown in the Figure 6. The aim is therefore to obtain a-SiN_x:H films with a refractive index between 2.0-2.4 (at 2 eV) while keeping the extinction coefficient as low as possible. Generally the extinction coefficient at 3.44 eV is considered, as for higher photon energies the transmission through the solar cell encapsulation material (glass with ethylene-vinyl acetate (EVA) foil) drops to zero [10]. This goal can be reached by the deposition of relatively N-rich films (to obtain low absorption) at a relatively high atomic film density (to obtain a sufficiently high refractive index). Furthermore, the film density and refractive index also plays an important role in obtaining the required degree of bulk passivation (as discussed below).

A possibility to obtain a high film density at relatively low substrate temperatures is the application of external substrate biasing. Due to the low electron temperature in the ETP plasma, the self bias at the substrate is very low and therefore there is no significant ion bombardment of the substrate. However, a controllable level of ion bombardment can be obtained by the application of lf or rf power to the substrate. This external substrate biasing has been explored in an industrial type of ETP reactor for a-SiN_x:H films deposited from an Ar-NH_3-SiH_4 plasma at substrate temperatures <150°C using different starting conditions for the rf and lf case [11]. As shown in Figure 7, the increase in film density with increasing dc bias voltage is clearly observed. This increase can, for a large part, be attributed to additional N incorporation into the film while no influence of the dc bias on the deposition rate has been observed.

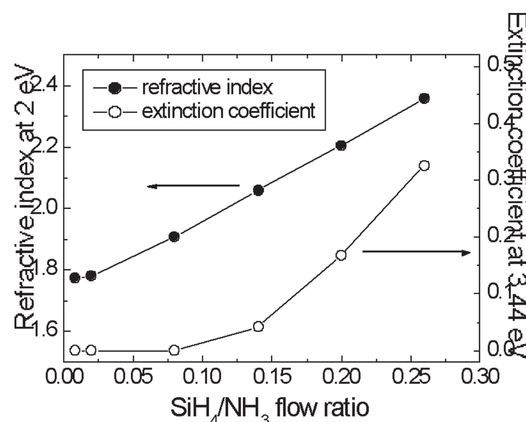

a.

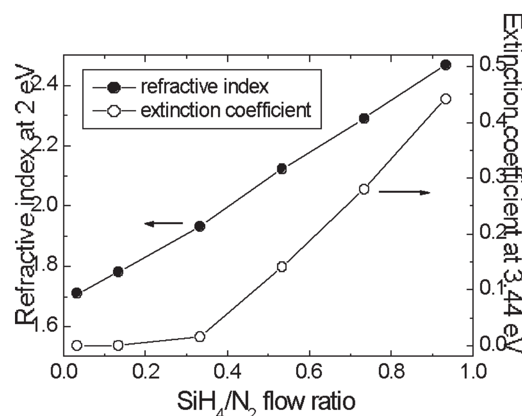

b.

Figure 6: Refractive index (at 2 eV) and extinction coefficient (at 3.44 eV) for different flow ratios of a.) SiH_4 and NH_3, and b.) SiH_4 and N_2.

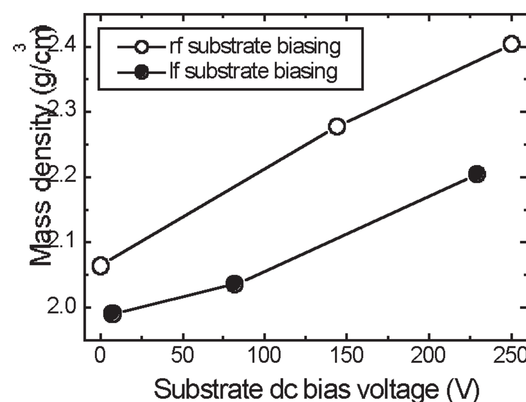

Figure 7: Mass density of a-SiN_x:H films as a function of the substrate bias. The films have been deposited at a temperature of <150°C.

As mentioned above, an a-SiN_x:H antireflection coating does not only reduce the optical losses but it can also provide surface and bulk passivation of the solar cells. For solar cells of mc-Si with screen printed contacts and a highly doped emitter, surface passivation is not yet an important issue, however, bulk passivation of the cells by the hydrogen released from the a-SiN_x:H layer can enhance the efficiency of the solar cells by ~15% (relative). This means that the efficiency of a typical mc-Si solar cell with an TiO_2 ARC can be increased from ~12.0-12.5% to approximately 14% by the application of an a-SiN_x:H ARC. This efficiency can be raised further (to an efficiency over 15%) by using a lower doping level for the emitter and by applying surface texture for better light trapping, etc.

To study whether such an enhancement in efficiency can be achieved by an a-SiN_x:H ARC deposited at high rate by the ETP technique, several lab-scale experiments have been carried out. First, it has been verified that a good ARC performance can be obtained by a-SiN_x:H films deposited from both the N_2-SiH_4 and NH_3-SiH_4 reactant mixture. As shown in Sec. 3, the optical properties of the film are fully tunable by the plasma conditions and for mc-Si solar cells (with a size of 10 x 10 cm^2) it has been shown that the reflectivity can be minimized using ETP a-SiN_x:H (using both reactant mixtures) with the right combination of refractive index and film thickness [6]. The results by Hong et al. [6] are similar to those obtained by state-of-the-art a-SiN_x:H films deposited by a remote microwave (MW) plasma at a rate of <1 nm/s. The fact that the a-SiN_x:H deposited from the Ar-H_2-N_2-SiH_4 plasma acts as a good ARC has also been proven by the production of laboratory c-Si solar cells (with a size of 2 x 2 cm^2). Due to the a-SiN_x:H ARC, the efficiency of the optimized cells increased from 12.8% to 18.1%, mainly due to the increase in short-circuit current [see Kessels et al., 6]. This gain in efficiency is only slightly lower than the reference cells coated with an rf parallel plate capacitively coupled plasma which also induce a high degree of surface passivation [6].

After establishing the ARC performance of the ETP deposited a-SiN_x:H, it has been tested whether the a-SiN_x:H films also induce bulk passivation. Therefore, solar cells produced from mc-Si wafers from the adjacent positions in the ingot have been coated by a-SiN_x:H films using the two different reactant mixtures. Furthermore, reference cells have been produced using state-of-the-art a-SiN_x:H deposited from a remote MW NH_3-SiH_4 plasma and by producing “reverse scenario cells” [6]. Because the lab-scale experiments on 10 x 10 cm^2 cells do not lead to a good uniformity, the bulk passivation is measured by local internal quantum efficiency (IQE) measurements as shown in Figure 8. The cells with a-SiN_x:H deposited from both the N_2-SiH_4 reactant mixture and NH_3-SiH_4 reactant mixture (see Figure 8), showed an increase in the IQE at near-infrared wavelengths compared to the reverse scenario cell. This so-called enhanced “red-response” indicates that bulk passivation is achieved. For the a-SiN_x:H deposited from the NH_3-SiH_4 reactant mixture, the increase is almost as high as for the state-of-the-art MW plasma deposited a-SiN_x:H, while the N_2-SiH_4 reactant mixture leads to a lower degree of bulk passivation. This is, therefore, a proof-of-principle that demonstrates that bulk passivation can be obtained by a-SiN_x:H deposited by the ETP at high rate and that the NH_3-SiH_4 reactant mixture is favored over the N_2-SiH_4 reactant mixture. Further optimization can take place in an industrial type reactor which yields good film uniformity (see below).

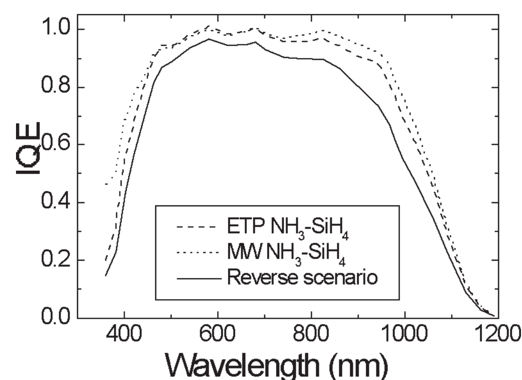

Figure 8: Internal quantum efficiency (IQE) of three solar cells with an a-SiN_x:H antireflection coating. The solar cells have been produced from mc-Si wafers from adjacent positions of an ingot. The ETP and microwave (MW) plasma deposited a-SiN_x:H have undergone the firing process while for the reverse scenario cell the a-SiN_x:H film has been deposited after the firing process.

On the basis of the aforementioned results, the ETP technique has been implemented for the deposition of a-SiN_x:H antireflection coatings on c-Si solar cells. The Netherlands based company, OTB Engineering B.V., has combined the technique with their sophisticated linear motion carrier technology such that an in-line deposition system is obtained which enables high volume production of a-SiN_x:H coated solar cells with a minimum amount of production line footprint. The deposition system, shown schematically in Figure 9, is called DEP_x and consists of a loadlock-in, heating zone, deposition zone, cooling zone and loadlock-out in a rectangular track. The carriers with solar cells are propelled electromagnetically through the different zones using motors which are located outside the vacuum. The deposition zone is a single process chamber which typically has three ETP plasma sources which run on the Ar-NH_3-SiH_4 gas mixture. The plasma source design has been optimized in terms of robustness and easy-maintenance and have only one single cathode each (see Figure 10). The a-SiN_x:H films deposited have an excellent uniformity of ±2.5% over the carrier width of 30 cm. The carriers hold 2 x 2 solar cells with a size of 15 x 15 cm^2 each. The nominal throughput of the DEP_x is 960 cells/hour and the total footprint of the system is 8 m^2, a combination that is only

feasible because of the high deposition rate of the ETP technique.

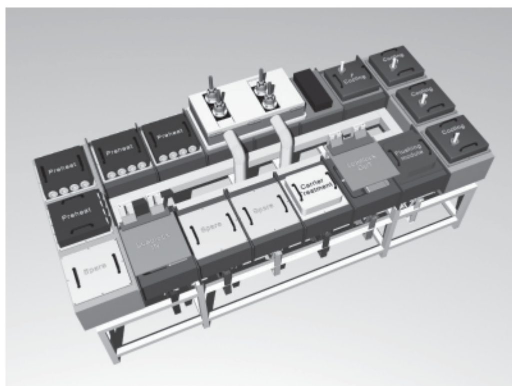

Figure 9: The DEP_x in-line production system for a-SiN_x:H deposition on solar cells. The deposition zone typically comprises three or four ETP plasma sources.

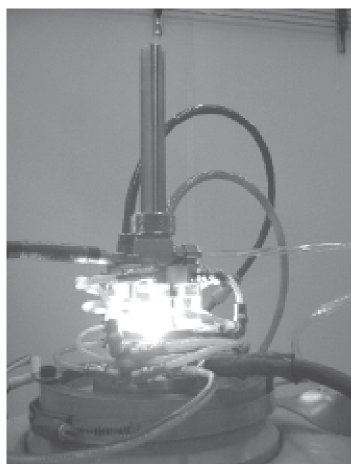

Figure 10: Picture of the redesigned ETP plasma source which is optimized in terms of reliability and easy maintenance.

With the DEP_x a-SiN_x:H films with a high mass density have been deposited and they induce a good degree of bulk passivation (even better than that obtained with the first industrial prototype reactor, see Hong et al. [6]) especially when considering the high deposition rates obtained. This has resulted in an increase in efficiency of mc-Si solar cells from 12.5% with a TiO_2 ARC to an efficiency of 14.4% for mc-Si solar cells with a-SiN_x:H ARC deposited with the DEP_x system. Recently, the first DEP_x has been installed in the new solar cell production line (with a capacity of 10 MW) at the Shell Solar facilities in Gelsenkirchen (Germany).

CONCLUSION

Two successful implementations of the novel ETP technology have been discussed, scratch resistant films on polycarbonate substrates and antireflection and bulk passivation layers on multicrystalline silicon solar cells. It has been shown that high quality thin films can be grown at high growth rate conditions (> 5nm/s). Although not specifically addressed in this article, much of the results have been enabled by the fundamental knowledge of the high rate deposition process, results which have been reported elsewhere, see for example Reference 12.

ACKNOWLEDGMENTS

The authors gratefully acknowledge B. Hoex, A.J.M. van Erven, F.J.H. van Assche, J.H. van Helden, M. van Hest, Y. Barrell, and Dr. R. Engeln for their contribution to the experiments. Parts of this study have been carried out within the E.E.T.-program "HR-CEL" and "Sunovation" funded by the Netherlands Ministry of Economic Affairs, the Ministry of Education, Culture and Science and the Ministry of Public Housing, Physical Planning and Environment. General Electric is thanked for their financial contribution to the Eindhoven research group. The research of W.K. has been made possible by a fellowship of the Royal Netherlands Academy of Arts and Sciences (KNAW).

REFERENCES

1. M.C.M. van de Sanden, R.J. Severens, W.M.M. Kessels, R.F.G. Meulenbroeks, and D.C. Schram, J. Appl. Phys 84, 2426 (1998); W.M.M. Kessels, M.G.H. Boogaarts, J.P.M. Hoefnagels, D.C. Schram, and M.C.M. van de Sanden, J. Vac. Sci. Technol. A 19 1027 (2001).

2. J.W.A.M. Gielen, W.M.M. Kessels, M.C.M. van de Sanden, and D.C. Schram, J. Appl. Phys. 82, 2643 (1997); J.W.A.M. Gielen, M.C.M. van de Sanden, and D.C. Schram, Appl. Phys. Lett. 69, 152 (1996).

3. R. Groenen, J.L. Linden, H.R.M. van Lierop, D.C. Schram, A.D. Kuypers, and M.C.M. van de Sanden, Appl. Surf. Sci. 173 40 (2001); R. Groenen, J. Löffler, P.M. Sommeling, J.L. Linden, E.A.G. Hamers, R.E.I. Schropp, and M.C.M. van de Sanden, Thin Solid Films 392 226 (2001).

4. D. C. Schram and G. M. W. Kroesen, U.S. Patent No. 4,871,580 (1989); European Patent No. 0297637 (1992).

5. M. Creatore, M.F.A.M. van Hest, J.Benedikt, and M.C.M. van de Sanden, MRS proc. 715, 101 (2002), M.Creatore, M. Kilic, K. O'Brien, R.Groenen, and M.C.M. van de Sanden, Thin Solid Films 427, 137 (2003); M.F.A.M. van Hest, B. Mitu, D.C. Schram, and M.C.M. van de Sanden, Thin Solid Films 449 52 (2004), Y. Barrell, M. Creatore, M. Schaepkens, C.D. Iacovangero, T. Miebach, and M.C.M. van de Sanden, Surf. Coat. Technol., 180-181 367 (2004).

6. W.M.M. Kessels, J. Hong, F.J.H. van Assche, M.D. Moschner, T. Lauinger, W.J. Soppe, A.W. Weeber, D.C. Schram, and M.C.M. van de Sanden, J. Vac. Sci. Technol. A 20, 1704 (2002), J. Hong, W.M.M. Kessels, W. J. Soppe, A.W. Weeber, W.M. Arnoldbik, and M.C.M. van de Sanden, J. Vac. Sci. Technol. B 21, 2123 (2003); J. Hong, W.M.M. Kessels, F.J.H. van Assche, H.C. Rieffe, W.J. Soppe, A.W. Weeber, and M.C.M. van de Sanden, Prog. Photovolt: Res. Appl. 11, 125 (2003).

7. M. Schaepkens, S. Selezneva, P. Moeleker, and C.D. Iacovangelo, J. Vac. Sci. Technol. A 21, 1266 (2003).

8. A. de Graaf, M.F.A.M. van Hest, M.C.M. van de Sanden, K.G.Y. Letourneur, and D.C. Schram, Appl. Phys. Lett. 74, 2927 (1999).

9. P. Doshi, G.E. Jellison, and A. Rohatgi, Appl. Opt. 36, 7826 (1997).

10. H. Nagel, A.G. Aberle, and R. Hezel, Prog. Photovolt: Res. Appl. 7, 245 (1999).

11. F.J.H. van Assche, W.M.M. Kessels, R. Vangheluwe, W.S. Mischke, M. Evers, and M.C.M. van de Sanden, submitted for publication (2004).

12. W.M.M. Kessels, A.H.M. Smets, D.C. Marra, E.S. Aydil, D.C. Schram, and M.C.M. van de Sanden, Thin Solid Films 383 154 (2001); J.P.M. Hoefnagels, A.A.E. Stevens, M.G.H. Boogaarts, W.M.M. Kessels, and M.C.M. van de Sanden, Chem. Phys. Lett. 360 189 (2002); W.M.M. Kessels, D.C. Marra, M.C.M. van de Sanden, and E.S. Aydil, J. Vac. Sci Technol. A 20 781 (2002); A.H.M. Smets, W.M.M. Kessels, and M.C.M. van de Sanden, Appl. Phys. Lett. 82 865 (2003); A.H.M. Smets, W.M.M. Kessels, and M.C.M. van de Sanden, Appl. Phys. Lett. 82 1547 (2003).